# Methodology for studying strain inhomogeneities in polycrystalline thin films during in situ thermal loading using coherent x-ray diffraction

Nicolas Vaxelaire, Henry Proudhon, S. Labat, C. Kirchlechner, J. Keckes, V. Jacques, S. Ravy, Samuel Forest, O. Thomas

New Journal of Physics
The open-access journal for physics

# Methodology for studying strain inhomogeneities in polycrystalline thin films during *in situ* thermal loading using coherent x-ray diffraction

**N Vaxelaire[1,2,6], H Proudhon[3], S Labat[1,2], C Kirchlechner[4], J Keckes[4], V Jacques[5], S Ravy[5], S Forest[3] and O Thomas[1,2]**

[1] Aix-Marseille University, IM2NP, FST avenue Escadrille Normandie Niemen, F-13397 Marseille Cedex, France
[2] CNRS, IM2NP, FST avenue Escadrille Normandie Niemen, F-13397 Marseille Cedex, France
[3] MINES ParisTech, Centre des matériaux, CNRS UMR 7633, BP 87, 91003 Evry Cedex, France
[4] Erich Schmid Institute for Material Science, Austrian Academy of Science and Institute of Metal Physics, University of Leoben, Jahnstrasse 12, 8700 Leoben, Austria
[5] Synchrotron SOLEIL, L'Orme des merisiers, Saint-Aubin BP 48, 91192 Gif-sur-Yvette Cedex, France
E-mail: nicolas.vaxelaire@univ-cezanne.fr

*New Journal of Physics* **12** (2010) 035018 (12pp)
Received 7 December 2009
Published 31 March 2010
Online at http://www.njp.org/
doi:10.1088/1367-2630/12/3/035018

**Abstract.** Coherent x-ray diffraction is used to investigate the mechanical properties of a single grain within a polycrystalline thin film *in situ* during a thermal cycle. Both the experimental approach and finite element simulation are described. Coherent diffraction from a single grain has been monitored *in situ* at different temperatures. This experiment offers unique perspectives for the study of the mechanical properties of nano-objects.

[6] Author to whom any correspondence should be addressed.

## Contents



## 1. Introduction

Coherent diffraction patterns from crystals in the Bragg mode are a fingerprint of the crystal shape but are also very sensitive to internal displacement fields [1]. This sensitivity to strain has been demonstrated in a few examples so far [2, 3]. Fundamental issues related to the ability to invert the three-dimensional (3D) diffraction pattern are still debated but chances are that it may become a unique way to image non-destructively strain fields with a resolution better than 10 nm. Impressive results can also be obtained with electron holography [4] but this requires sample thinning, which may drastically modify the initial strain field. Thus, imaging strain fields by coherent x-ray diffraction at the nanometer scale opens interesting possibilities in the field of mechanics in small dimensions.

The development of heterogeneous deformation within polycrystals remains an important research topic in the field of mechanics. In the past 15 years, significant advances have been obtained by combining numerical simulations with experimental measurements of displacement fields. The former rely on the finite element (FE) method and continuum crystal elasto-plasticity, whereas the latter are derived from digital image correlation or lattice rotation fields measured by EBSD at the micrometer scale [5, 6]. It has been shown that grain boundaries are sources of strong strain incompatibilities in the case of anisotropic elasticity, even in mainly ⟨111⟩ oriented grains in thin films and coatings [7]. Strain heterogeneities become even more pronounced when plasticity occurs. In the sub-micrometer range the lack of appropriate techniques to investigate strains at these scales prevents any comparison of simulations with experiments.

In the present work, we show that coherent x-ray diffraction is a promising tool to investigate the detailed intragranular displacement field within a polycrystalline aggregate. FE modeling is used to derive the displacement field, which in turn allows calculating the diffraction pattern from the deformed grain. First we describe the general methodology (section 2) that has been used in the present work: preparation of Au polycrystalline samples and characterization of the structure and average thermo-mechanical properties. Section 3 addresses the issue of numerical simulation from FE modeling of the displacement field to the 3D calculation of coherent diffraction patterns from deformed grains. Section 4 is devoted to the actual coherent x-ray diffraction measurements from crystals within polycrystalline aggregates. Experimental

results are discussed and compared with numerical simulations. A final conclusion synthesizes the major findings and discusses perspectives and directions for future work.

## 2. Methodology: samples and characterization

The sample studied here is a polycrystalline gold thin film, 375 nm thick, deposited on a glass substrate. Gold presents two interesting advantages: it has a high scattering factor and it does not easily oxidize. The sample was annealed in flame for a few seconds at 800–900 °C. The in-plane typical size of the grains lies between 0.200 and 3 $\mu$m.

Some preliminary characterization of the sample has been performed with a conventional x-ray source. The laboratory measurement was made in a high-resolution mode with a beam divergence around 0.007°. A hybrid optic composed of a parabolic multi-layer mirror followed by a two-reflection Ge ⟨220⟩ channel cut was used to monochromatize the beam. The $K_\alpha$ line from the copper anti-cathode was selected with a dispersion around 1 eV. The sample was mounted on the center of rotation of a four-circle goniometer. Finally, for strain measurement, the diffracted signal was recorded with a proportional counter after a three-reflection Ge ⟨220⟩ channel cut used as an analyzer.

The film presents a strong ⟨111⟩ texture (figure 1(a)). However, the ⟨111⟩ grains present some mosaicity (full-width at half-maximum (FWHM) of 3.6°) (figure 1(b)). In the plane of the film, the grains are randomly oriented. Indeed the $[\bar{1}11]$ direction of the different grains is distributed on a circle on the ⟨111⟩ pole figure (figure 1(c)).

The mechanical loading was performed via heating up and cooling down the sample. Because glass and gold thermal expansion coefficients are different, a strain field is induced in the thin film during heating (see equation (1)). In the different experiments explained here, the sample was heated up to 450 °C:

$$\epsilon_{//} = \left[\alpha_{SiO_2}\Delta(T) - \alpha_{Au}\Delta(T)\right]. \tag{1}$$

The furnace was previously calibrated with MgO powder[7]. At each temperature, a long exposure $\theta 2\theta$ scan was collected. The $2\theta$ position was then derived from a fit of the diffraction peak with a pseudo-Voigt function. This position of the peak gives the precise $d_{111}$ parameter perpendicular to the film. Then perpendicular strain is calculated from the temperature-dependent [8] lattice parameter of Au, given by equation (2):

$$a_{Au}(T_i) = a_0\left[1 + \int_{25}^{T_i} \alpha(T)\,\mathrm{d}(T)\right]. \tag{2}$$

The in-plane strain is finally deduced from the out-of-plane strain using the assumption of zero out-of-plane stress:

$$\frac{\epsilon_{//}}{\epsilon_{\perp}} = -\eta_{111},$$

where

$$\eta_{111} = 2\frac{C_{11} + 2C_{12} - C_{44}}{C_{11} + C_{12} + 4C_{44}}$$

(see [9]). The numerical value is around 1.245 for gold [10]. The theoretical out-of-plane thermo-elastic strain is compared to the experimental one in figure 1(d).

[7] MgO is well suited to perform calibration thanks to its large thermal expansion coefficient.

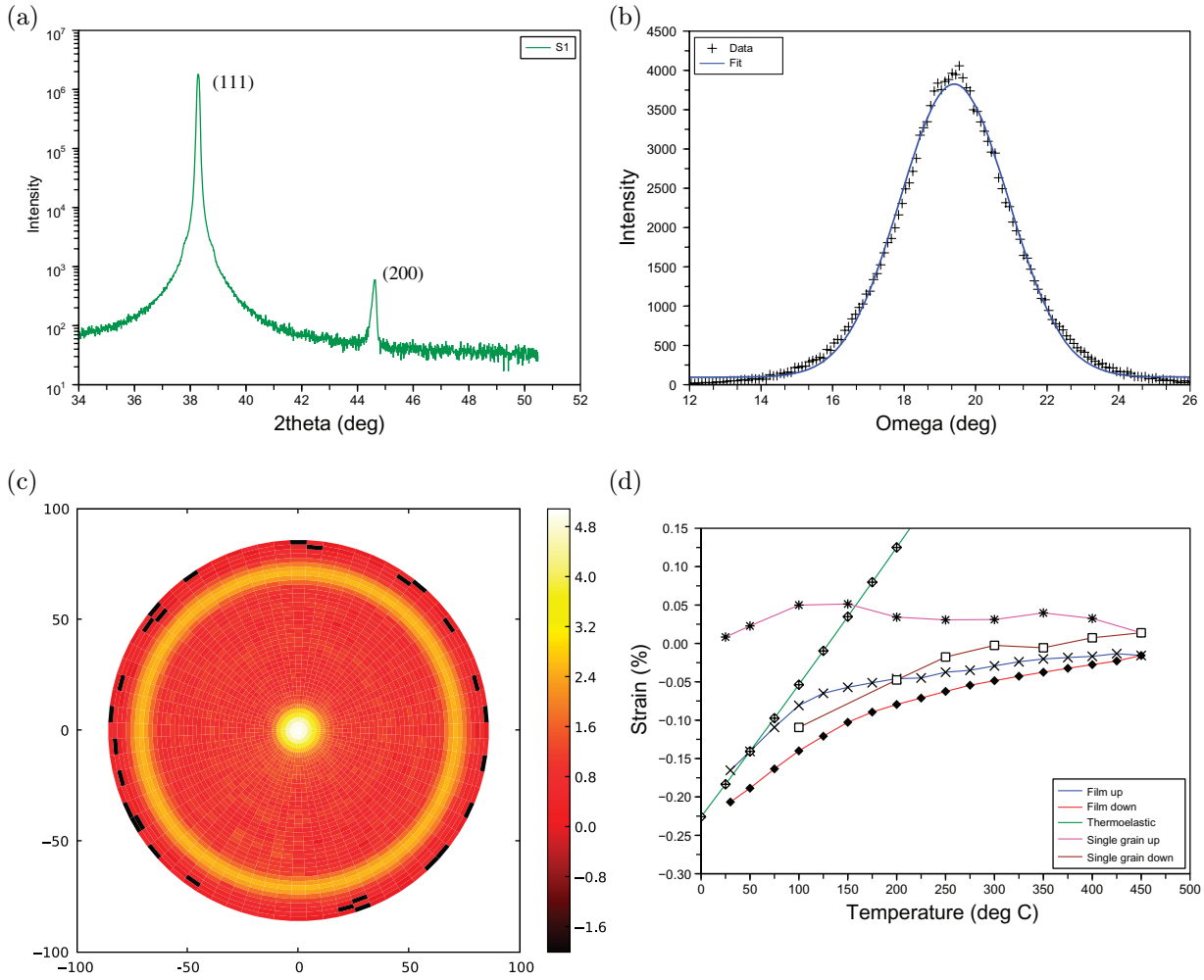


**Figure 1.** Sample characterization with a lab setup and Cu $K_\alpha$ radiation. These texture and strain versus temperature measurements concern a large number of Au grains. In (d) single grain measurements from the shift of the coherent diffraction pattern are also shown. (a) Theta2theta scan, (b) Omega scan, (c) $\langle \bar{1}11 \rangle$ pole figure and (d) average perpendicular strain during the first thermal loading in lab.

The initial experimental slope is smaller than the thermo-elastic one. This might be explained by non-elastic behavior (grain boundary grooving for example) or possibly a lack of adhesion of the film to the substrate. The experimental thermal cycle is opened and presents a flat portion at high temperatures. This behavior is indicative of plastic relaxation.

It should be emphasized that these measurements represent the second thermal cycle. The first thermal cycle concerns the *in situ* coherent diffraction experiment. The coherent diffraction to be described in section 3 was performed on polycrystalline features patterned with a focused ion beam (FIB) in the Au thin film. Ten-micron-sized squares in the middle of 150 $\mu$m bare substrate areas were prepared in order to get a finite size polycrystal containing 133 grains. Such a number of grains can be directly implemented in simulations. Thus we have the same boundary conditions in the simulated polycrystal and in the experiment.

## 3. Numerical simulation of coherent diffraction

Finite element simulations of the behavior of polycrystalline aggregates have not yet been used to interpret diffraction patterns. The objective of the present section is to show that the detailed intragranular displacement field predicted by 3D FE computations can be exploited to delineate the respective effects of grain shape, orientation and strain on the evolution of complex diffraction patterns.

### *3.1. Theoretical aspects*

Within the framework of the kinematic theory of diffraction[8], the 3D intensity produced by a coherent beam diffracted by a small crystal is expressed as the sum of the complex amplitude scattered by each atom:

$$I(\mathbf{q}) \propto \left| \sum_n f_n(\mathbf{q}) \exp(\mathrm{i}\mathbf{q}\mathbf{r}_n) \right|^2 \tag{3}$$

with $\mathbf{r}_n$ being the atomic position at $n$ and $f_n$ being its scattering factor.

For a deformed crystal, we define $\mathbf{u}(x, y, z)$ as the displacement vector field, which is the difference between the current and initial atom positions. Hence, $\mathbf{r}_n = x\mathbf{a} + y\mathbf{b} + z\mathbf{c} + \mathbf{u}(x, y, z)$ with $x$, $y$ and $z$ being integer values and $\mathbf{a}$, $\mathbf{b}$ and $\mathbf{c}$ being the basis vectors of the perfect crystal lattice.

With the scattering vector written in the reciprocal space ($\mathbf{A}$, $\mathbf{B}$, $\mathbf{C}$), equation (3) becomes

$$I(\mathbf{q}) \propto \left| \sum_{xyz} f_n(\mathbf{q}) \exp\left(\mathrm{i}\mathbf{u}(x, y, z) \cdot \mathbf{q}\right) \exp\left(\mathrm{i}2\pi(hx + ky + lz)\right) \right|^2. \tag{4}$$

Considering pure metals, $f_n$ does not depend on $n$. Within the Takagi approximation [11] and with $\mathbf{q} = \mathbf{G} + \Delta\mathbf{q}$, equation (4) can be rewritten with a Fourier transform if $\Delta\mathbf{q} \ll \mathbf{G}$:

$$I(\mathbf{q}) \propto |TF\{\rho(\mathbf{r}) \cdot \exp(\mathrm{i}\mathbf{G} \cdot \mathbf{u}(\mathbf{r}))\}|^2. \tag{5}$$

Thus intensity $I(\mathbf{q})$ is evaluated using the displacement field computed by finite element analysis within a polycrystal model.

### *3.2. Numerical simulation of a 3D coherent diffraction pattern*

To compute the strain heterogeneities within a polycrystalline sample, a suitable mesh of the grains must be obtained. A standard way to mesh a polycrystal is to use Voronoi tessellations in two or three dimensions. This has been used successfully in the past to simulate the mechanical behavior of thin copper films [12], but real grain geometry can also be used favorably if available [13]. In this work, thanks to their columnar nature, the precise shape of the grains can be extracted from a scanning electron microscopy (SEM) image in back scattered electron mode (which provides some crystalline contrast), as shown in figure 2. The resulting 2D microstructure is then extended in the $Z$-direction to obtain the 3D mesh with 133 grains.

[8] This assumption is valid because of the small reflected intensity compared to incident beam (large rocking curve ($\simeq 0.3^\circ$)).

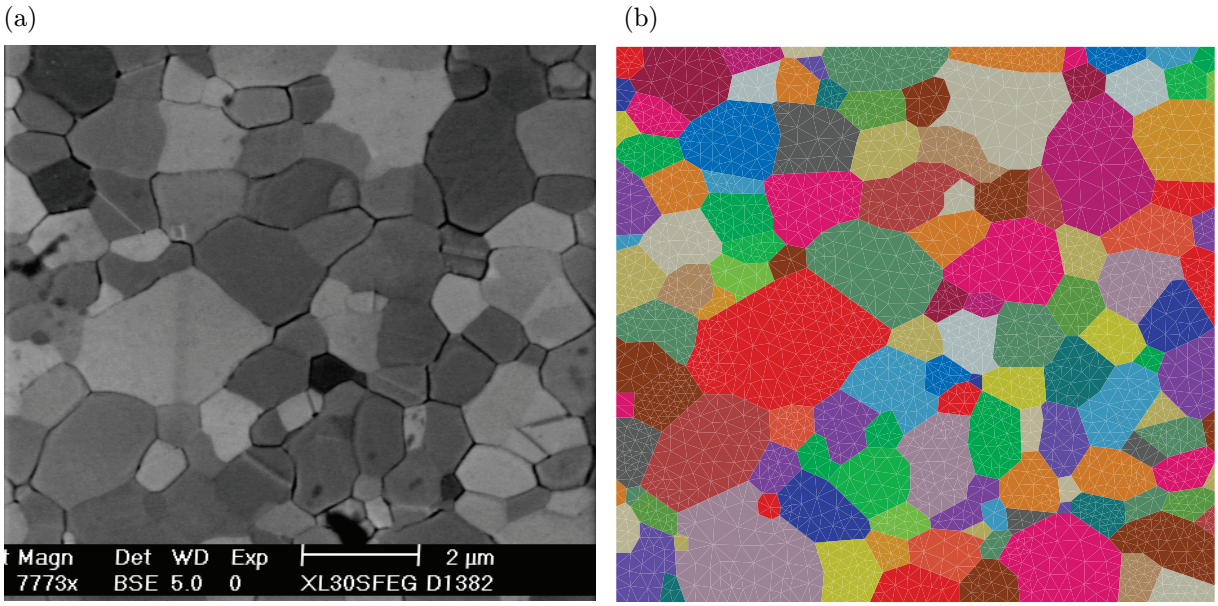


**Figure 2.** Extraction of the surface grain topology (a) SEM image of isolated polycrystal and (b) Grain topology extracted from the SEM image.

The mesh closely matches the gold sample size of $10 \times 10 \times 0.2\,\mu\text{m}^3$. As the exact orientations of the grains were not available at the time of the computations, a fiber texture with $\langle 111 \rangle$ parallel to the surface and random in-plane orientation is applied. To match as closely as possible the experimental orientation set, small deviations of the $\langle 111 \rangle$ direction are taken into account. These deviations are applied randomly within the experimental scatter, as measured on the lab x-ray diffractometer.

FEM calculations were performed using $Z$-SeT software suite[9] using linear elasticity behavior with cubic anisotropy to represent the gold crystal network. The following elastic constants $C_{ij}$ have been used [10]: $C_{11} = 192\,340$ MPa, $C_{12} = 163\,140$ MPa and $C_{44} = 41\,950$ MPa. For face centered cubic (FCC) crystals, the Bragg vector is $\mathbf{G}_{hkl} = 2\pi/a[h, k, l]$ with $a$ the atomic spacing taken as $a = 0.4078$ nm. The effect of temperature on these parameters is neglected.

The different steps chained to obtain the 3D diffraction pattern in a selected grain are shown in figure 3. Starting with the 3D mesh and the grain orientation set (figure 3(a)), boundary conditions are applied (sample fixed on the lower face to simulate a rigid glass substrate and a temperature change of $\Delta T = 100$ K applied linearly over time (figure 3(b)). The FEM calculation is carried out to retrieve the heterogeneous stress and strain fields (figure 3(c)). The displacement field $\mathbf{u}(x, y, z)$ is then transferred to a regular mesh (typically $200 \times 200 \times 5$ elements; figure 3(d)). Finally, equation (5) is computed with a complex FFT[10]. on a $200^3$ array filled with zero outside the grain and with $\{\cos(2\pi/a(hu_x + ku_y + lu_z)), \sin(2\pi/a(hu_x + ku_y + lu_z))\}$ inside the selected grain. The amplitude of the complex output is stored into a 3D data set, which can then be visualized in the reciprocal space $(q_x, q_y, q_z)$ and further analyzed (figure 3(e)).

[9] Available at http://www.nwnumerics.com.
[10] Computations were based on FFTW version 3.2.1 [14].

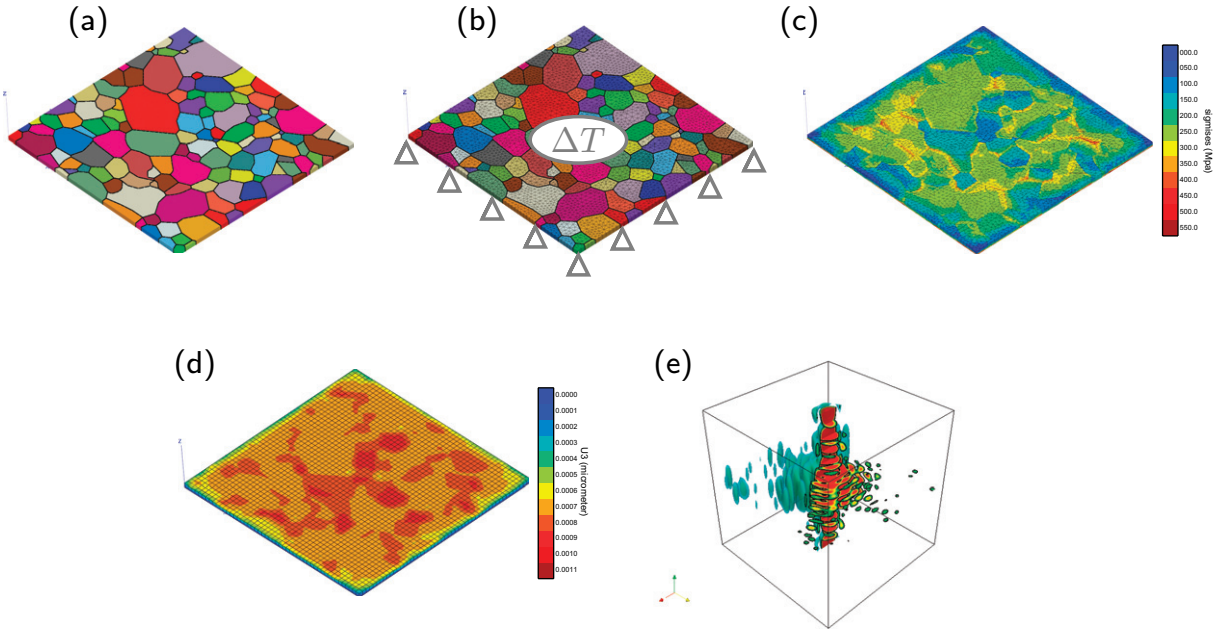


**Figure 3.** Illustration of the methodology used to compute the 3D diffraction pattern on a selected grain within a polycrystalline microstructure. (a) 3d topology and orientations, (b) 3d mesh with boundary conditions, (c) heterogeneous von Mises stress field, (d) displacement field transfered on regular mesh and (e) 3d diffraction pattern for selected grain.

### *3.3. Application to a selected grain*

The numerical diffraction procedure has been used with a particular grain named grain#52 in the following, and the results are presented in figure 4. In the first column, no deformation has been applied yet, so that the diffraction pattern shows the effect of the shape only. One can see a symmetric pattern (FFT with a real input). Subsequent thermal straining clearly introduces some strain heterogeneities (see von Mises stress contours) and the diffraction pattern deforms and progressively loses its symmetry.

By simulating the heterogeneous displacement field in a polycrystal, one can easily change a variety of parameters like grain shape and/or orientation, level of strain, boundary conditions, etc. Tying those computations with FFT can provide a very useful tool to understand the complexity of the real 3D coherent diffraction pattern observed experimentally.

## 4. Experimental results

### *4.1. Beamline setup*

To perform coherent x-ray diffraction, third generation synchrotron light sources are required. The experiments have been performed at the CRISTAL beamline of the SOLEIL synchrotron. This beamline is well suited for coherent diffraction measurements. The source is a U20 undulator located 36 m upstream of the sample. The beam is monochromatized by a double Si(111) crystal. The number of windows along the beam is reduced to 1 to avoid coherence perturbations [15].

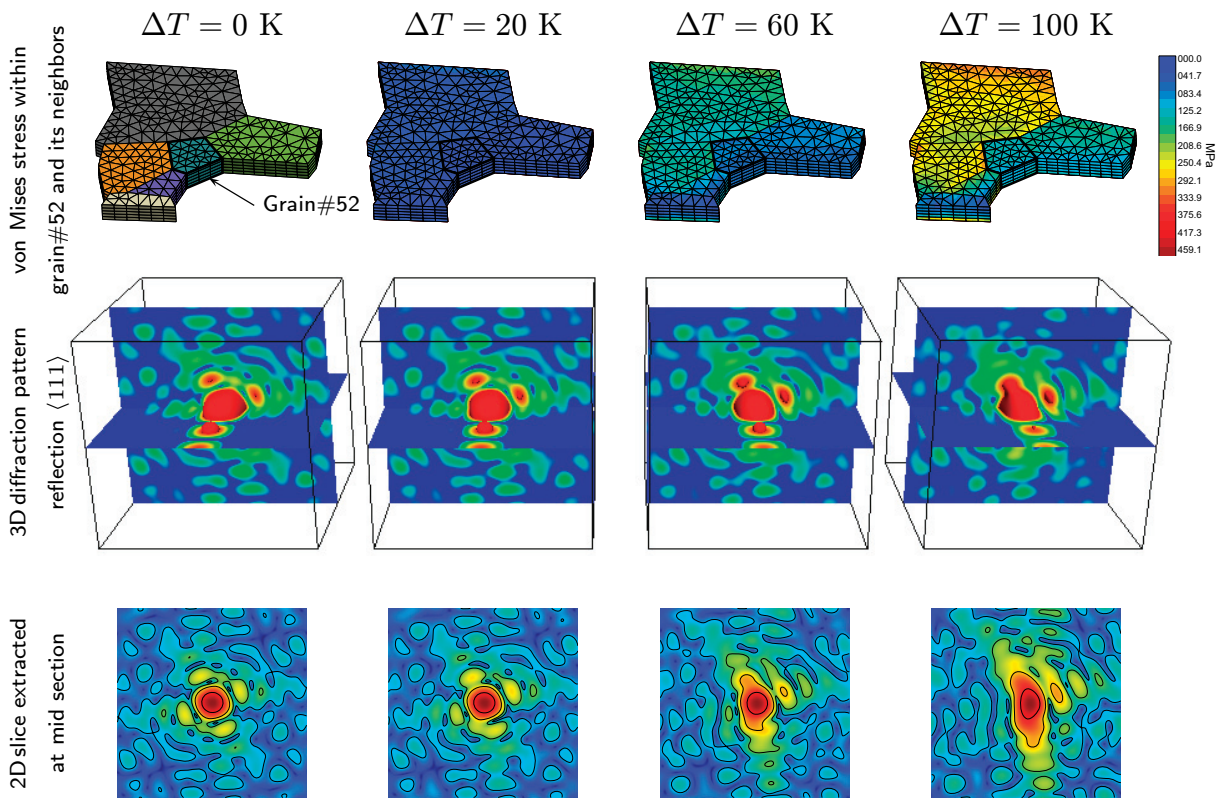


**Figure 4.** Simulation of coherent diffraction in grain#52 at different strain levels; the top panel depicts the heterogeneous von Mises stress field in grain#52 and some of its neighbors, the middle panel shows the simulated 3D diffraction pattern visualized by means of a contour surface and two orthogonal slices, bottom panel shows slices extracted from the diffraction pattern at $q_z = 0$.

The goal of the experiment was to record the Bragg intensity from a single grain and at the same time to know which grain was diffracting in order to perform FE simulation. To reach this goal, a special design of the sample was made. A $10 \times 10\,\mu\text{m}^2$ polycrystal was isolated at the center of a $150 \times 150\,\mu\text{m}^2$ region where the initial gold thin film was etched by FIB[11].

The shaping of the beam was achieved by slits located 15 cm before the sample. The optimum aperture of these slits was calculated in order to obtain the smallest beam footprint on the sample [16]. According to the diffraction angle projection[12], the beam was $5 \times 25\,\mu\text{m}^2$. The beam size was sufficient to see the region without gold and hence find the polycrystal. To ensure finding the region, the fluorescence signal of the gold was recorded thanks to a specific energy dispersive detector[13]. To collect this fluorescence it is necessary to bring the energy above the $L_3$ gold absorption edge, which is excited for an energy up to 11.91 keV. The fluorescence map was very convenient to locate the region of interest (figure 5).

To collect the Bragg signal a direct illuminated CCD camera from Andor with $1024 \times 1024$ pixels of $13 \times 13\,\mu\text{m}^2$ is used. The detector is positioned on a $2\theta$ arm at around 1.2 m from the

[11] Zeiss 1540 XB.
[12] $1/(\sin(12^\circ)) \simeq 5$.
[13] Rontec fluorescence detector.

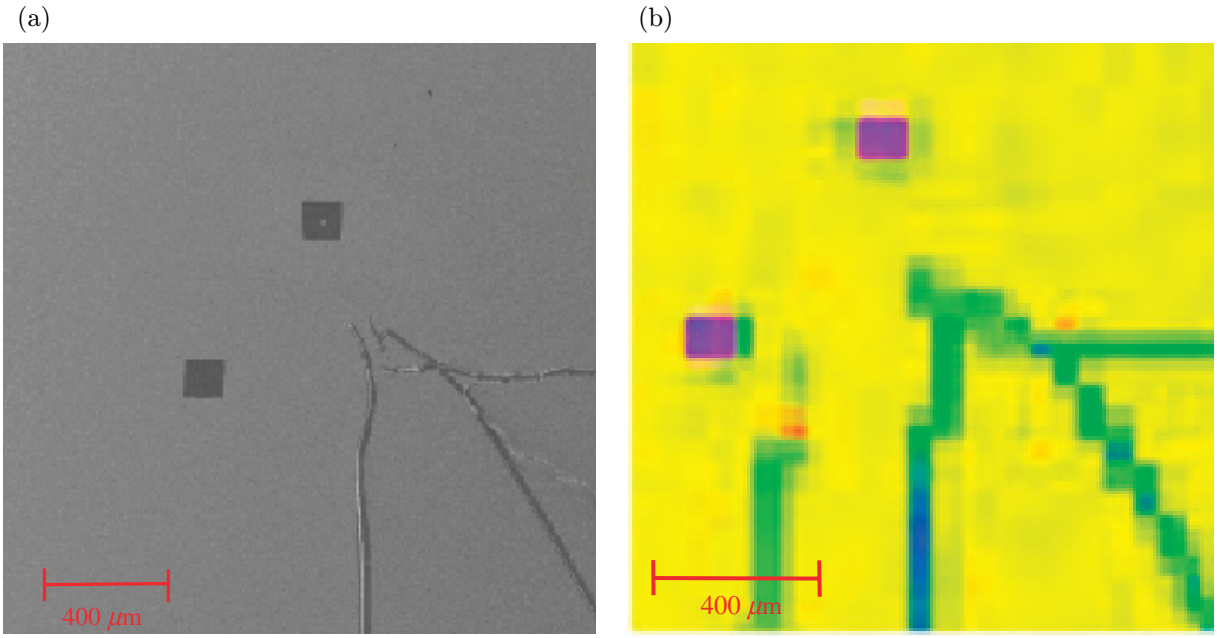


**Figure 5.** The special design of the sample allows us to find the isolated polycrystal thanks to fluorescence mapping. (a) SEM image of the sample surface and (b) fluorescence scan.

sample to obtain a good resolution in direct space. A flight tube was used to limit absorption by air. The experimental noise was reduced by cooling down the CCD and by working in a single photon mode thanks to droplet algorithm [17]. This algorithm reduced the spreading of photons on the pixels and it is reasonable to neglect the convolution pixel effect. The resolution in these working conditions reached in the plane of the CCD camera was:

$$\delta q_{\mathrm{Del,Nu}} \simeq \frac{1}{\lambda} \cdot \frac{\mathrm{Size_{Pixel}}}{L} \simeq 1.098^{-4}\,\mathrm{nm}^{-1}.$$

### *4.2. Experimental measurements*

Once the coherent diffraction pattern from a single grain inside the isolated polycrystal was recorded, a thermal cycle was performed. (111) Bragg reflection in a coplanar symmetric geometry was recorded. A rocking curve was performed every 50 °C. A long exposure 200 × 2 s 2D slice was taken at the maximum of the rocking curve for each temperature step. Typically the long exposure acquisition yields a total count of $4 \times 10^6$ photons on the CCD with a maximum of around 7000 photons on one pixel.

A uniform strain simply shifts in $2\theta$ the Bragg peak. On the other hand, distortion of the diffraction pattern is related to inhomogeneous strains (i.e. at least a power 2 law for the displacement field). In brief, the average strain in the grain is related to the global shift of the diffraction pattern whereas the distortion of the pattern, is related to the strain variation within the grain. The 3D center of gravity of the peak was monitored at every temperature. The results are summarized in figure 1(d). On that plot, one can compare the individual and the collective behavior. The single grain is mildly sensitive to loading during the heating up. However, during

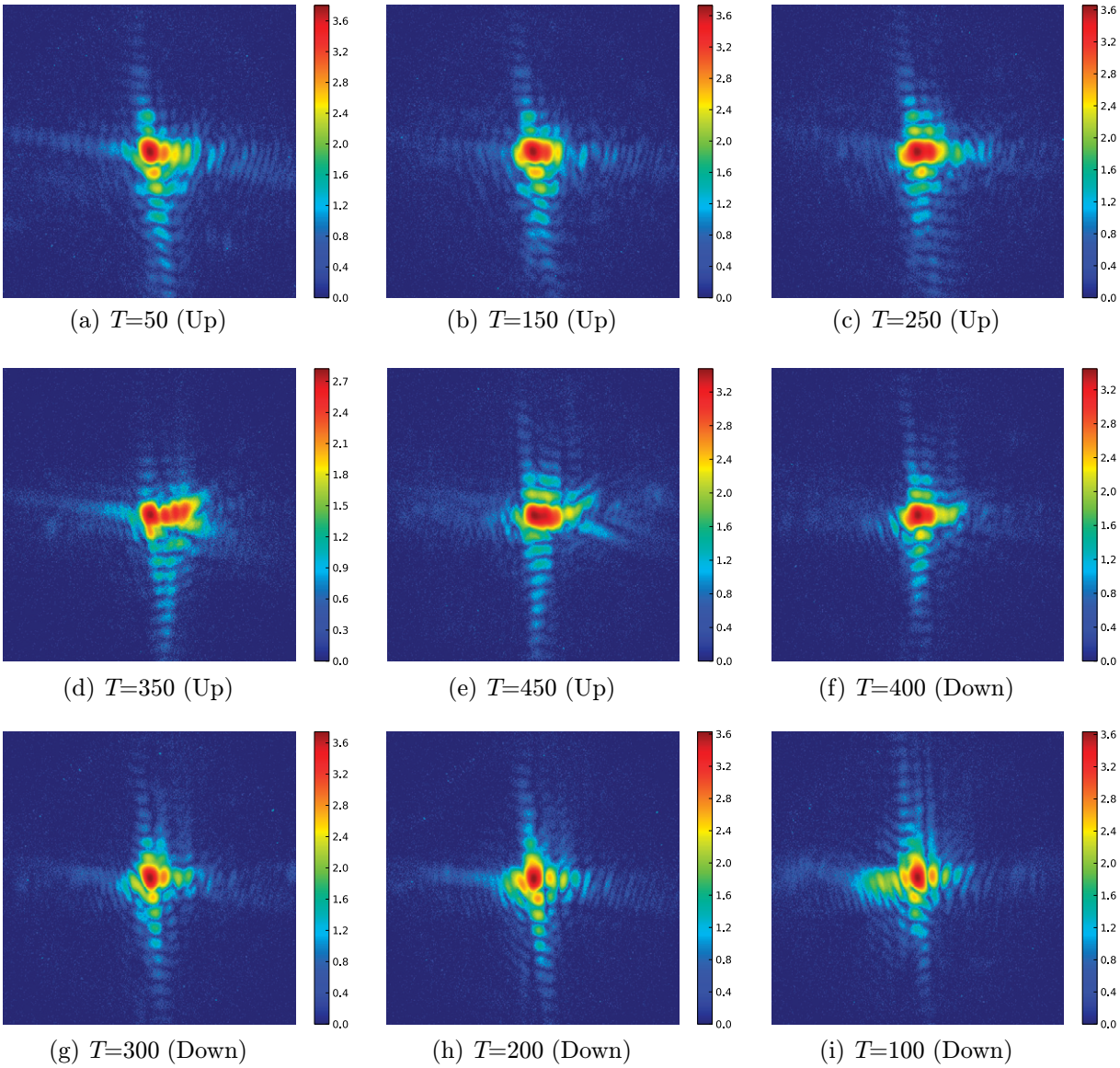

(a) $T$=50 (Up) (b) $T$=150 (Up) (c) $T$=250 (Up)

(d) $T$=350 (Up) (e) $T$=450 (Up) (f) $T$=400 (Down)

(g) $T$=300 (Down) (h) $T$=200 (Down) (i) $T$=100 (Down)

**Figure 6.** Evolution of the 2D slice taken at the maximum of rocking during the first thermic cycle (log10 scale).

cooling down its average strain is going down, and the grain is under tension. One should note that the cycle performed at the SOLEIL beamline was the first one and the cycle performed on the laboratory source was the second one.

Qualitatively, a strong effect on diffraction pattern is observed during the thermal loading (figure 6). A split of the center of the peak appears for a temperature around 300 °C. During the cooling down, the central splitting disappears but an irreversible behavior change in the peak shape is observed. Indeed, the fringes are different from the initial ones. This irreversible behavior may be related to plastic activity.

In our working conditions, oversampling reaches 24 × 16 in the plane of the CCD, which means that fringes are described by 24 and 16 points for the two main directions. Direct space

dimensions of the diffracting grain have been deduced and are $380 \times 570\,\text{nm}^2$. 380 nm is in good agreement with the expected film thickness. A quantitative mapping of the displacement field requires inversion procedures, which will be used on these data. This data treatment consists in retrieving the phase of the wavefield that is lost on the detector provided that some constraints about data acquisition are verified, which is the case here [18]. To reach this goal, several algorithms have been developed [3], [19]–[23].

## 5. Conclusion and perspectives

In this work, we have shown temperature-dependent coherent diffraction measurements. Single grain coherent diffraction patterns from an Au polycrystal have been recorded at different temperatures. The change of these patterns with temperature is related to the evolution of strains within the grain. Finite element modeling shows qualitatively similar behavior.

This work will develop in several directions. First, we expect that very soon we will be able to fully invert the diffraction patterns and thus get a complete strain mapping as a function of temperature. Moreover, our experimental findings indicate that plasticity probably plays a role even at low temperatures. Finite element plasticity will clearly be needed in order to get a better understanding of the coherent diffraction patterns.

Recent improvements in detectors (pixel detectors) will allow collecting 3D Bragg peaks faster and will be very useful for *in situ* characterization, allowing us to collect more than three independent Bragg reflections for each temperature. On the other hand, the constant improvement of light sources (focalization, flux, etc) would allow performing measurements further in reciprocal space, and thus improve the resolution in direct space possibly down to 5 nm.

## Acknowledgments

The financial support of ANR-08-JCJC-0095-01 is gratefully acknowledged.

## References

[1] Robinson I and Harder R 2009 Coherent x-ray diffraction imaging of strain at the nanoscale *Nat. Mater.* **8** 291–8

[2] Pfeifer M A, Williams G J, Vartanyants I A, Harder R and Robinson I K 2006 Three-dimensional mapping of a deformation field inside a nanocrystal *Nature* **442** 63–6

[3] Minkevich A A, Gailhanou M, Micha J-S, Charlet B, Chamard V and Thomas O 2007 Inversion of the diffraction pattern from an inhomogeneously strained crystal using an iterative algorithm *Phys. Rev.* B **76** 104106

[4] Hytch M, Houdellier F, Hue F and Snoeck E 2008 Nanoscale holographic interferometry for strain measurements in electronic devices *Nature* **453** 1086–9

[5] Delaire F, Raphanel J L and Rey C 2000 Plastic heterogeneities of a copper multicrystal deformed in uniaxial tension: experimental study and finite element simulations *Acta Mater.* **48** 1075–87

[6] Zeghadi A, N'Guyen F, Forest S, Gourgues A-F and Bouaziz O 2007 Ensemble averaging stress–strain fields in polycrystalline aggregates with a constrained surface microstructure—Part 1: Anisotropic elastic behaviour *Phil. Mag.* **87** 1401–24

[7] Šiška F, Forest S and Gumbsch P 2007 Simulation of stress–strain heterogeneities in copper thin films: texture and substrate effects *Comput. Mater. Sci.* **39** 137–41

[8] Touloukian Y S, Kirby R K, Taylor R E and Desai P D 1976 *Thermal Expansion* vol 12 (New York: Plenum)
[9] Nye J F 1957 *Physical Properties of Crystals—Their Representation by Tensors and Matrices* (Oxford: Oxford Science Publications)
[10] Neighbours J R and Alers G A 1958 Elastic constants of silver and gold *Phys. Rev.* **111** 707–12
[11] Takagi S 1969 A dynamical theory of diffraction for a distorted crystal *J. Phys. Soc. Japan* **26** 1239–53
[12] Šiška F, Forest S, Gumbsch P and Weygand D 2007 Finite element simulations of the cyclic elastoplastic behaviour of copper thin films *Model. Simul. Mater. Sci. Eng.* **15** S217–38
[13] Parisot R, Forest S, Gourgues A F, Pineau A and Mareuse D 2001 Modeling the mechanical behavior of a multicrystalline zinc coating on a hot-dip galvanized steel sheet *Comput. Mater. Sci.* **19** 189–204
[14] Frigo M and Johnson S G 2005 The design and implementation of FFTW3 *Proc. IEEE* **93** 216–31 (special issue on 'Program Generation, Optimization and Platform Adaptation')
[15] Robinson I K, Kenney-Benson C A and Vartanyants I A 2003 Sources of decoherence in beamline optics *Physica* B **336** 56–62
[16] Born M and Wolf E 1959 *Principles of Optics* (Oxford: Pergamon)
[17] Livet F, Bley F, Mainville J, Caudron R, Mochrie S G J, Geissler E, Dolino G, Abernathy D, Grubel G and Sutton M 2000 Using direct illumination CCDs as high-resolution area detectors for x-ray scattering *Nucl. Instrum. Methods Phys. Res.* **451** 596–609
[18] Sayre D 1952 Some implications of a theorem due to Shannon *Acta Crystallogr.* **5** 843
[19] Gerchberg R W and Saxton W O 1972 Phase determination from image and diffraction plane pictures in the electron microscope *Optik* **35** 237–46
[20] Fienup J R 1982 Phase retrieval algorithms: a comparison *Appl. Opt.* **21** 2758–69
[21] Bauschke H H, Combettes P L and Luke D R 2003 Hybrid projection–reflection method for phase retrieval *J. Opt. Soc. Am.* A **20** 1025–34
[22] Millane R P 1990 Phase retrieval in crystallography and optics *J. Opt. Soc. Am.* A **7** 394–411
[23] Marchesini S 2007 Invited article: a unified evaluation of iterative projection algorithms for phase retrieval *Rev. Sci. Instrum.* **78** 011301